# Influence of Tabula Rasa on Process- and Light-Induced Degradation of Solar Cells Fabricated From Czochralski Silicon

Abigail R. Meyer [ID], Vincenzo LaSalvia, William Nemeth, Wanxing Xu [ID], Matthew Page, David L. Young [ID], Sumit Agarwal, and Paul Stradins [ID]

*Abstract*—Monocrystalline Si solar cells are fabricated from Czochralski (Cz) Si, which contains $10^{17}$–$10^{18}$ cm$^{-3}$ oxygen atoms. Cz Si undergoes degradation during high-temperature thermal processing steps, such as dopant diffusion to form the *p-n* junction. This degradation in the bulk minority carrier lifetime can be related to the formation of oxygen precipitates. We found that a high-temperature annealing process known as *tabula rasa* (TR) not only mitigates process-induced degradation via oxygen precipitate nuclei dissolution, but also modifies subsequent light-induced degradation. We report on the bulk carrier lifetime of *n*- and *p*-type Cz Si after TR, which homogenizes the interstitial oxygen in the bulk Si to its monoatomic form in either an $N_2$ or $O_2$ environment. A control sample, which was not subjected to a TR processing step, experienced severe process-induced degradation during a boron emitter thermal budget as oxygen precipitates were formed in the Si bulk. These precipitates could be imaged using photoluminescence. Additionally, samples that underwent a TR processing step prior to the boron emitter thermal budget show efficient gettering of metallic impurities compared to the control sample, which showed a decline in the implied open-circuit voltage after the gettering step. Furthermore, modification of the interstitial oxygen bonding by TR had a strong effect on the light-induced degradation kinetics. Instead of a typically observed monotonic decrease, minority carrier lifetime increases first, followed by a nonmonotonic decrease over a $\sim$20 h period. We conclude that by modifying the interstitial oxygen bonding via TR pretreatment, *p*-type Cz Si wafers become substantially resistant to harsh solar cell processes and strongly modified light-induced degradation, which would open alternative ways to mitigate this degradation mechanism.

*Index Terms*—Degradation, oxygen precipitation, silicon solar cell, tabula rasa.

Abigail R. Meyer is with the Department of Chemical and Biological Engineering, Colorado School of Mines, Golden, CO 80401 USA, and also with the National Renewable Energy Laboratory, Golden, CO 80401 USA (e-mail: abigailmeyer@mymail.mines.edu).

Vincenzo LaSalvia, William Nemeth, Matthew Page, David L. Young, and Paul Stradins are with the National Renewable Energy Laboratory, Golden, CO 80401 USA (e-mail: vincenzo.lasalvia@nrel.gov; william.nemeth@nrel.gov; matthew.page@nrel.gov; david.young@nrel.gov; pauls.stradins@nrel.gov).

Wanxing Xu and Sumit Agarwal are with the Department of Chemical and Biological Engineering, Colorado School of Mines, Golden, CO 80401 USA (e-mail: wanxingxu@mines.edu; sagarwal@mines.edu).

## I. INTRODUCTION

BORON-DOPED, *p*-type passivated emitter rear contact (*p*-PERC) Si solar cells are the fastest growing solar technology in the market today, with efficiencies reaching over 22% [1]. Due to the higher efficiencies of *p*-PERC solar cells, this architecture has replaced the aluminum back-surface field solar cell, which exhibits lower efficiencies due to high recombination at the rear of the cell [2]. The *p*-PERC architecture minimizes the Al to Si contact at the back of the cell, has a front shallow emitter, [3] and enhanced back reflection via a dielectric stack at the rear of the cell [4], [5]. These three features result in exceptional surface passivation leading to higher efficiencies. With these higher efficiencies in *p*-PERC solar cells, the bulk minority carrier lifetime $\tau_{\text{bulk}}$ becomes an important factor, and to maintain the high-efficiency of *p*-PERC cells, it is important to eliminate the bulk degradation pathways during cell processing especially during the high-temperature processes, and during cell operation, more specifically light-induced degradation (LID).

Monocrystalline Si solar cells are fabricated from Czochralski (Cz) Si. Since this growth process occurs in a quartz crucible, $10^{17}$–$10^{18}$ cm$^{-3}$ interstitial oxygen atoms are incorporated into Cz Si. During the manufacture of solar cells from these Cz Si wafers, high-temperature dopant diffusion is required to create a *p-n* junction. This step also leads to gettering of metal impurities in bulk Cz Si to the surface. Process-induced degradation occurs in Cz Si during this dopant diffusion step, which typically requires a temperature of $\sim$900 °C. During this high-temperature process, extended oxygen precipitates are formed from small clusters of interstitial oxygen interacting with vacancies and their agglomerates [6]. An oxygen precipitate is generally defined as a small particle of $SiO_x$ ($1 \leq x \leq 2$) [7]. These oxygen precipitates hinder the performance of the resulting cell [8], [9] by acting as gettering centers for metal impurities, and also act as recombination-active sites especially when they are decorated with Fe atoms [9]. Process-induced degradation can be mitigated in phosphorous-doped *n*-type Cz Si

through a high-temperature annealing step referred to as *tabula rasa* (TR) [10], which literally means "clean slate" in Latin. However, there have been minimal studies on how TR can be employed to mitigate the process-induced degradation in *p*-type Si [11], [12]. In addition to the process-induced degradation, *p*-type Cz Si is also prone to LID, which can cause ∼2% relative efficiency loss in *p*-PERC cells [13]. The mechanism for LID is generally well accepted and involves the formation of a complex consisting of a substitutional boron atom $B_s$ and an oxygen dimer $O_{2i}$ [14]. As a result, the extent of defect creation in LID scales quadratically with the interstitial oxygen content [15]. In 2006, Herguth *et al.* discovered a technological solution to LID called "regeneration" [16], which has since been implemented into industrial production [17]. Given that the TR treatment influences the interstitial oxygen bonding configuration in Cz Si [11], it is not clear how such a treatment, if incorporated into manufacturing, would in turn influence the kinetics or extent of LID. It has already been shown by Bothe *et al.* that high temperature thermal processes can alter LID by up to a factor of three [18].

In Cz Si, oxygen and carbon are the two impurities with the highest number density. In addition, Cz ingots also have intrinsic defects such as vacancies and Si interstitials [19]. The thermal history of a Cz Si wafer after the Cz growth process determines the formation, or lack thereof, of oxygen precipitates. It has been shown that in Cz Si, the density of oxygen precipitation depends on the annealing time and temperature [20], [21]. The annealing behavior can be divided into three temperature ranges: <800 °C, 800–1050 °C, and >1050 °C, which dictate weather oxygen precipitate nuclei will grow or annihilate. If, prior to device fabrication, there is a low-temperature preannealing step, 2–10 h at 750 °C, oxygen precipitate nuclei will form in large quantities and increase in size, many exceeding a critical radius to grow at higher temperatures. As the wafers are heated to higher temperatures [22]–[24] of ∼800–1000 °C following the preannealing step, oxygen precipitation rate increases along with the precipitate density with lower temperatures within this range resulting in a faster precipitate formation with increased density [20]. This increase in oxygen precipitation rate is a result of the oxygen precipitate nuclei growing during the preannealing step, and when heated to higher temperatures the nuclei can grow further and not annihilate. Additionally, oxygen precipitation depends on the ambient gas used during annealing over the temperature range of ∼800–1000 °C, with an oxygen ambient resulting in reduced oxygen precipitate growth and an inert ambient resulting in increased oxygen precipitate growth [25], [26]. Finally, a short, high-temperature preanneal at ≥1050 °C has been shown to inhibit oxygen precipitate formation kinetics in subsequent thermal steps [20], [24]. This retardation in oxygen precipitate formation is attributed to the breakup of the nuclei responsible for subsequent precipitate formation. Note, if this short, high-temperature anneal is conducted after lower temperature anneals, it is expected that oxygen precipitate nuclei have grown during the lower temperature steps and oxygen precipitation would allow for the development of lifetime-limiting precipitates. These oxygen precipitate nuclei have been loosely identified as vacancy clusters [20], silicon-interstitial-enriched

swirl defects [24], oxygen clusters, or small dislocation loops that trap interstitial oxygen [27], [28]. The latter two defect structures are considered the primary candidates for the nuclei that lead to larger $SiO_x$ particles. These defects are created at temperatures below 800 °C and above 1200 °C, but are unstable in the intermediate temperature range of 1000–1200 °C [27]. The short, high-temperature (>1050 °C) preannealing treatment described above is sometimes referred to as "*tabula rasa*," and allows for the manipulation of intrinsic defects incorporated during the Cz growth process, and suppresses oxygen precipitation in Cz Si.

*Tabula rasa* treatment of *n*-type Cz Si prevents degradation of $\tau_{\text{bulk}}$ and the lowering of the implied open-circuit voltage ($iV_{\text{oc}}$) that is otherwise observed after the thermal processing step for the fabrication of the boron emitter. TR also enables the gettering of metal impurities to the surface in *n*-type Cz Si [6], [29]. This improvement in $\tau_{\text{bulk}}$ is attributed to annihilation of oxygen precipitate nuclei during TR, as discussed above [29]. During TR, most of the oxygen atoms within the Cz Si bulk are able to take on the isolated interstitial form due to breaking up of oxygen precipitate nuclei and oxygen clusters that act as thermal donors [30]. Similar to oxygen precipitate formation, the ambient during TR also influences subsequent process-induced degradation. It has been shown that in *n*-type Cz Si [6] and upgraded metallurgical-grade Si [29], TR conducted prior to a thermal treatment step, which is equivalent to the dopant diffusion step, resulted in a higher $iV_{\text{oc}}$ if the TR step was in an $O_2$ ambient compared to an $N_2$ ambient. While the influence of TR is better understood for solar cells fabricated from *n*-type Cz Si [6], [10], [29], there are only a few studies on the influence of TR on solar devices fabricated from *p*-type Cz Si [19], [31]. A majority of the studies on mitigation of process-induced degradation due to oxygen precipitates in *p*-type Cz Si have been for integrated circuit manufacturing [32], [33].

In this article, we investigate how implementing different durations of TR treatments in $O_2$ and $N_2$ ambient, prior to a dopant diffusion step, affects process-induced degradation in *p*-type Cz Si. We also study how adding a TR processing step affects subsequent gettering of metal impurities to the surface. Finally, we investigate the influence of a TR processing step on the kinetics of LID in *p*-type Cz Si.

## II. EXPERIMENTAL DETAILS

### A. Wafer Preparation

Low- (2.2 Ω·cm) and high-resistivity (23 Ω·cm) 156 mm, *p*-type Cz-Si wafers were obtained from Woongjin Energy and Jinko Solar, respectively. *n*-type wafers with a resistivity of 3.7 Ω·cm were also obtained from Woongjin Energy. Each wafer was scribed into four 60 × 60 mm pieces from the center of the wafer with their edges along the {1 0 0} direction, and rest of the wafer edges were discarded. Low-resistivity *p*-type, high-resistivity *p*-type, and *n*-type samples had interstitial oxygen concentrations of $6.7 \times 10^{17}$, $8.8 \times 10^{17}$, and $5.6 \times 10^{17}$ cm$^{-3}$, respectively, based on the intensity of the infrared vibrational mode at 1107 cm$^{-1}$ measured using transmission Fourier transform infrared spectroscopy [34]. The saw-damage on the wafer
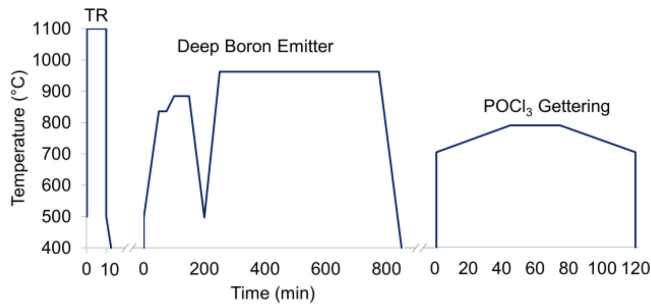
Fig. 1. Schematic showing the thermal annealing steps used for all samples in this study, including TR treatment, deep boron emitter creation, and POCl$_3$ gettering. The TR treatment was also performed on one quarter of each of the wafers for 30 min instead of 10 min.

surface was removed in 22.5% aqueous KOH solution for 15 min followed by dipping into a 1% aqueous HF/HCl (6:1) solution for 10 min to remove the residual potassium. The wafers were then cleaned using piranha, RCA-1, and RCA-2, which are standard wafer cleaning procedures, followed by a treatment with 1.7% aqueous HF solution to remove the $SiO_x$ formed as a result of cleaning [35], [36]. Immediately after cleaning, the resistivity of the wafer pieces was measured using a 4-point probe, and these values are quoted above. The $iV_{oc}$ was measured with a Sinton lifetime tester while the surface was passivated by immersing the wafers in a 10% aqueous HF/HCl (6:1) liquid passivation. The as-received low-resistivity $p$-type Cz Si, high-resistivity $p$-type Cz Si, and the $n$-type Cz-Si samples had $iV_{oc}$ values of 700 ± 10, 735 ± 5, 735 ± 5 mV, respectively.

### B. Tabula Rasa Treatment

Three of the four pieces from each individual Si wafer were subjected to annealing in a tube furnace. The samples were loaded into a quartz boat and inserted into a furnace preheated to a temperature of 1100 °C with ∼1 atm ambient gas pressure. A different TR process was used for each of the three Si pieces from each wafer: annealing in (a) an O$_2$ ambient for 10 min, (b) an O$_2$ ambient for 30 min, and (c) an N$_2$ ambient for 10 min (see Fig. 1). After the annealing duration, the quartz boat was pulled out of the furnace, and the wafers were cooled under atmospheric conditions. Subsequently, the thermal oxide formed on the surface was stripped in HF and $\tau_{bulk}$ was measured with a Sinton lifetime tester using liquid passivation as described in Section II-A. The wafer resistivities were measured again with a 4-point probe after the TR treatment. The resistivities of low- and high-resistivity $p$-type wafers decreased to ∼1.7 and ∼8.5 Ω·cm, respectively, while that of the $n$-type wafers increased to ∼5.3 Ω·cm. This change in resistivities is consistent with the breakup of small interstitial oxygen clusters [37] that act as thermal donors [38]. The fourth Si piece from each wafer was not subjected to a TR treatment, and acts as reference. Henceforth, this piece will be referred to as the "control sample."

To determine the effectiveness of the TR treatment in mitigating process-induced degradation, all samples were subject to a high-temperature annealing step that mimicked the formation of a deep boron emitter. During this thermal treatment, no dopants

were diffused into the samples. We term this thermal treatment as a "boron budget" (BB) (see Fig. 1). This BB was ∼800 min long at ∼900 °C. Subsequently, the samples were recleaned using the process described above. This was followed by passivation of the surfaces with ∼15 nm of Al$_2$O$_3$ deposited with atomic layer deposition using trimethyl aluminum and water as precursors. After Al$_2$O$_3$ growth, the samples were annealed in forming gas for 20 min at 400 °C. These samples were analyzed via a Sinton lifetime tester to determine $\tau_{bulk}$ and $iV_{oc}$. The degradation of the samples was also determined using a photoluminescence (PL) imaging setup, which uses laser diodes and a GaAs filter to measure the emission due to radiative recombination at a set illumination intensity under steady-state conditions [39]. The PL fluorescence of each sample was quantified with ImageJ software. Finally, the Al$_2$O$_3$ film was removed in a 10% HF solution and the wafers were recleaned prior to POCl$_3$ gettering. Gettering was conducted at 785° C with a 30 min dwell time (see Fig. 1). The phosphosilicate glass and the resulting doped region in Si were removed with 10% HF and 22.5% KOH, respectively. $\tau_{bulk}$ was again measured using the Sinton lifetime tester with the sample surface passivated in a HF/HCl solution, as described in Section II-A.

### C. Light-Soaking and Dark-Annealing

Light-soaking to induce LID and subsequent dark-annealing was conducted at room temperature for 24 h at an illumination intensity of 100 mW/cm$^2$ (commercial tungsten halogen lamp) calibrated with a silicon solar cell, and at 200 °C for 20 min in the dark, respectively. $\tau_{bulk}$ was measured after each step using the Sinton lifetime tester, and reported for an injection level of 10$^{15}$ cm$^{-3}$ for low-resistivity boron-doped samples and 2.5 × 10$^{14}$ cm$^{-3}$ for high-resistivity boron-doped samples which corresponds to $\Delta n = 0.48 \times p_0$, where $\Delta n$ is the excess carrier concentration and $p_0$ is the number of boron acceptors.

## III. RESULTS AND DISCUSSION

### A. Effect of Tabula Rasa Annealing Ambient on Bulk Minority Carrier Lifetime

Fig. 2 shows the bulk minority carrier lifetime as a function of the injection level for both (a) low- and (b) high-resistivity $p$-type samples for the three TR treatment conditions described in Section II-B along with the control sample. For both low- and high-resistivity samples, we observed a decrease in $\tau_{bulk}$ for samples that were subjected to a N$_2$ ambient TR treatment, while for samples subjected to TR in an O$_2$ ambient $\tau_{bulk}$ increased when compared to the control samples. This observation is consistent with previous studies conducted on $n$-type Cz Si, [6], [29] and can be explained based on the behavior of point defects in Cz Si during TR treatment. It is well known in the literature that during annealing of Cz Si at 1100 °C, Frenkel pairs (vacancy and interstitial pairs) are created spontaneously in the bulk at concentrations that are on the order of 10$^{18}$ cm$^{-3}$ (see Fig. 3) [40]. The Si interstitials diffuse much faster than the vacancies and a certain fraction of these interstitials can reach the surface of the wafer and get annihilated. When TR is conducted in a N$_2$
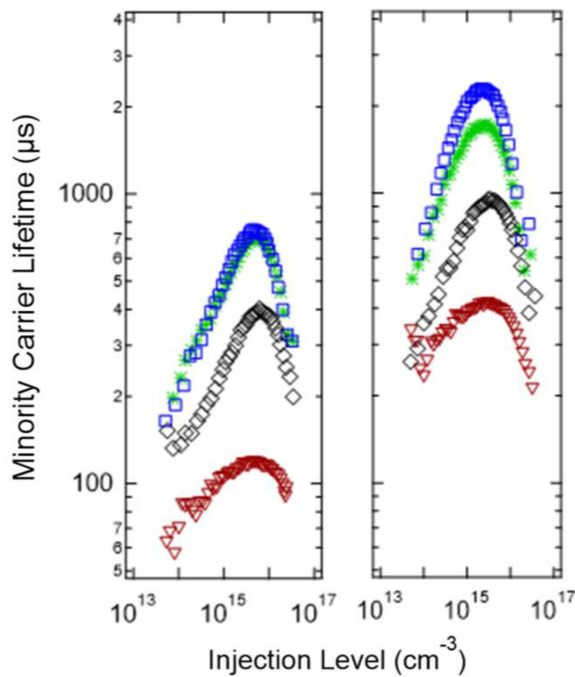
Fig. 2. Minority carrier lifetime as a function of the injection level recorded immediately after TR processing for the (a) 2.2 $\Omega \cdot$cm and (b) 23 $\Omega \cdot$cm resistivity $p$-type Cz Si samples. In each case, the three different TR processes including O$_2$ ambient for 30 min ($\square$), O$_2$ ambient for 10 min ($_*$), and N$_2$ ambient for 10 min ($\triangledown$). A control sample is also shown that did not undergo TR treatment ($\diamondsuit$).
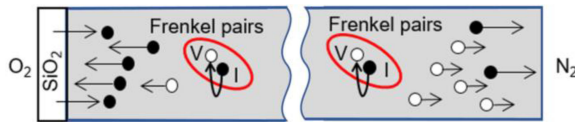


Fig. 3. Schematic of the atomistic-level mechanisms hypothesized to occur during TR treatment in an O$_2$ and N$_2$ ambient. The closed circles represent Si self-interstitials (I) and the open circles represent vacancies (V).

ambient, a steady-state concentration of vacancies accumulates in the bulk. When the samples are cooled rapidly, these vacancies are frozen in and act as recombination centers [41]–[43], which correlates with a decrease in $\tau_{bulk}$. When TR is conducted in an O$_2$ ambient, a $\sim$20-nm-thick SiO$_2$ film forms on the surface of the wafer. This oxidation causes stress near the Si/SiO$_2$ interface, resulting in a supersaturation of Si self-interstitials [44], [45]. These interstitials are injected into the bulk [44], [46], [47] and cause nucleation and growth of stacking faults near the surface [45]. These interstitials are also hypothesized to suppress the large vacancy concentration [48], [49] that would otherwise remain in an N$_2$ ambient in the absence of surface oxidation. This large concentration of interstitials is frozen into the lattice during cooling, but such interstitials are relatively benign compared to the recombination-active vacancies [40].

## B. Effect of Deep Boron Emitter Thermal Budget on Oxygen Precipitation

Fig. 4 shows PL images of high-resistivity $p$-type Cz Si, low-resistivity $p$-type Cz Si, and $n$-type Cz Si wafers that were

cut into four quarters and subjected to TR at different conditions followed by a thermal annealing step that replicates the boron emitter processing step (see Fig. 1). Hereafter, we refer to this annealing step as BB. In these PL images, the appearance of concentric ring structures would indicate the presence of oxygen precipitates [50], and a bright PL signature would indicate that the BB did not cause any significant degradation. The PL pixel intensity of each sample was quantified with ImageJ software. For samples where the BB caused severe process-induced degradation, the PL images appear dark. To detect if there were any ring-like structures formed in these samples due to oxygen precipitates, we increased the exposure time on the charged-coupled device (CCD) for the PL measurement by a factor of 12. All images that have a white arrow pointing to them with no text overlaid on the image were taken when exposure time on the CCD detector of the PL setup was increased by a factor of 12. High-resistivity $p$-type Cz Si samples annealed in O$_2$ or N$_2$ for 10 min resulted in a brighter PL image compared to samples annealed in O$_2$ for 30 min and the control sample [see Fig. 4(a)]. We attribute the decline in PL brightness in the sample annealed in O$_2$ for 30 min to contamination within bulk Si during processing or other phenomena not related to lifetime-limiting oxygen precipitation due to the absence of ring-like structures in the PL image when the CCD collection time was increased. A quarter of a ring-like band indicated by the dashed line does appear on the control sample in Fig. 4(a) after the incident light intensity was increased. We can therefore conclude that the decline in the PL brightness for this control sample was caused by process-induced degradation brought on by oxygen precipitation, and a TR step in N$_2$ or O$_2$ ambient allows for mitigation of process-induced degradation during a BB.

Fig. 4(b) and (c) shows the PL images of the low-resistivity $p$-type Cz Si and $n$-type Cz Si quarters, respectively, after the BB. Similar to the high-resistivity $p$-type Cz Si quarters, low-resistivity $p$-type Cz Si and $n$-type Cz Si quarters that were annealed in a N$_2$ or O$_2$ ambient have a brighter PL image compared to the control sample. When the collection time CCD was increased by a factor of 12 for the low-resistivity $p$-type Cz Si control sample, ring-like features appeared [see Fig. 4(b)] indicating the formation of oxygen precipitates. These ring-like structures could be observed for the control $n$-type Cz-Si sample in Fig. 4(c) without having to increase the incident light intensity during the PL imaging. Therefore, we can again conclude that either an N$_2$ or O$_2$ ambient during TR mitigates process-induced degradation in both $p$- and $n$-type Cz Si.

The results for the $n$-type Cz Si samples are similar to previous work by LaSalvia *et al.* who reported mitigation of process-induced degradation by TR performed in either an N$_2$ or O$_2$ ambient [6]. It is well known that oxygen precipitation is caused by a supersaturation of the interstitial oxygen concentration under the influence of point defects such as carbon, Si self-interstitials, and vacancies [19]. While oxygen, carbon, and vacancies are known to enhance the growth of oxygen precipitates, Si self-interstitials suppress their growth [19]. Oxygen precipitate nuclei are composed of a vacancy in the Si lattice with interstitial oxygen atoms in the vicinity of this vacancy. The TR processing step in both an O$_2$ and N$_2$ ambient retards oxygen precipitation during the BB
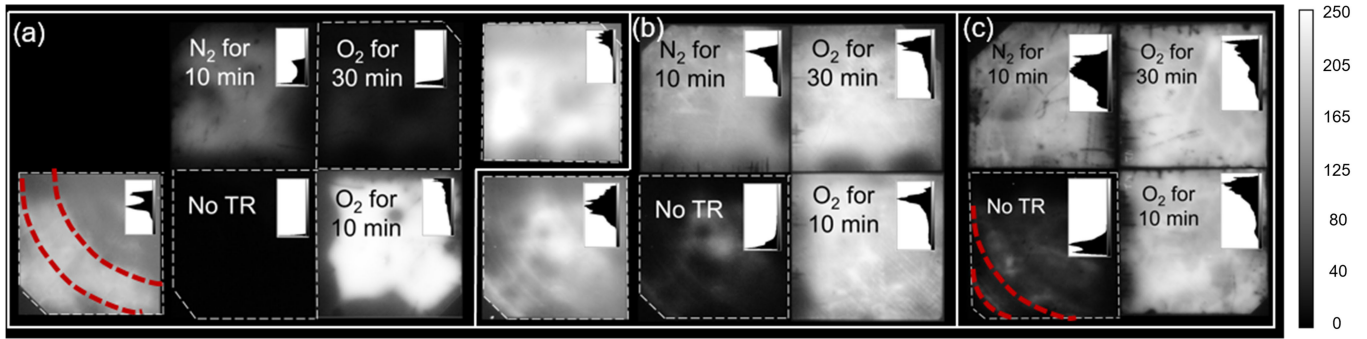
Fig. 4. PL images of (a) high resistivity *p*-type Cz-Si, (b) low resistivity *p*-type Cz-Si, and (c) *n*-type Cz-Si with various TR treatments noted on the PL image. These PL images recorded the deep boron emitter diffusion thermal budget. The quarters with an additional image have been photographed a second time with $12\times$ the CCD to reveal the oxygen precipitate rings. The dashed red lines indicate the ring-like structures that appear in the PL images due to the formation of oxygen precipitates. The pixel intensity in the PL images quantified with ImageJ software is shown as an inset in each image. In this scale, the top corresponds to the brightest pixel and the bottom corresponds to the darkest pixel with a full range from 0 to 250. The horizontal histograms show the distribution of the pixel intensities in each PL image. Therefore, the brightest images show a peak toward the top and the darker images show a peak at the bottom.
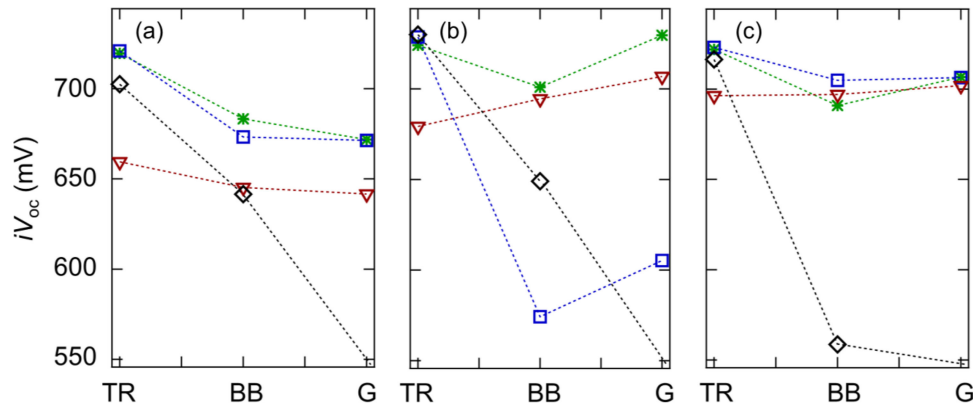


Fig. 5. $iV_{oc}$ for (a) low-resistivity *p*-type Cz Si, (b) high-resistivity *p*-type Cz Si, and (c) *n*-type Cz Si samples immediately after TR, after TR-treated samples were exposed to a BB, and after samples that underwent a BB were subjected to POCl$_3$ gettering (G). In each figure, the three different TR processes including O$_2$ ambient for 30 min ($\square$), O$_2$ ambient for 10 min ($*$), and N$_2$ ambient for 10 min ($\triangledown$). A control sample is also shown that did not undergo TR treatment ($\diamondsuit$).

by breaking up these oxygen precipitate nuclei at temperatures above 1000 °C. We generally observed a brighter PL image after the TR treatment in O$_2$ ambient compared to N$_2$ due to the injection of Si self-interstitials, which suppresses vacancies and further oxygen precipitation. It should be noted that N$_2$ ambient was used during the BB. If an O$_2$ ambient were to be used, oxygen precipitate nuclei may behave differently than an N$_2$ ambient.

### C. Effect of BB and POCl Gettering on $iV_{oc}$

The *n*-type doped surface layer formed in a POCl$_3$ environment is known to getter impurities, such as trace metals, to the surface of the wafer [51]. It is well known that oxygen precipitates also act as effective gettering sinks for transition metal impurities such as Fe that are present in the Si bulk [52], [53]. Therefore, it is expected that if oxygen precipitates are present in the Si bulk, when the wafer undergoes a POCl$_3$ gettering step, these oxygen precipitates will prevent efficient gettering of impurities to the surface of the Si wafer. Conversely, if no oxygen precipitates are present in the Si bulk during the POCl$_3$ gettering step, it is likely that impurities will be more

effectively gettered to the surface and subsequently etched away, resulting in an increase in $iV_{oc}$. Thus, $iV_{oc}$ is a good measure of the effectiveness of the TR step in mitigating process-induced degradation.

Fig. 5(a)–(c) shows the $iV_{oc}$ of the low-resistivity *p*-type Cz Si samples, high-resistivity *p*-type Cz Si samples, and *n*-type Cz Si samples, respectively, immediately after the TR step, after the TR-treated samples were subjected to the BB, and after the BB-treated samples were subjected to the POCl$_3$ gettering step (G). Fig. 5 includes samples that were annealed in O$_2$ ambient for 10 or 30 min, and samples that were annealed in N$_2$ ambient for 10 min. The $iV_{oc}$ value of samples that were not subject to a TR treatment step are also shown for comparison. In Fig. 5, for samples that were already subjected to TR treatment, after the BB step, there is a small decrease in $iV_{oc}$ for samples that were annealed in an N$_2$ or O$_2$ ambient. The only exceptions to this are the high-resistivity *p*-type Cz Si and the *n*-type Cz Si samples that were annealed in a N$_2$ ambient for 10 min. On the other hand, the control sample that did not undergo TR treatment shows a more drastic decrease in $iV_{oc}$, $\sim$50–100 mV, after the BB step. The high-resistivity *p*-type Cz Si samples annealed in O$_2$ for 30 min shows a decrease in $iV_{oc}$ that is greater than that for the control

sample. We attribute this not to the ineffectiveness of the TR step, but to contamination during processing (see Fig. 4(a) and the discussion in Section III-B). After subjecting low-resistivity $p$-type Cz Si samples to a $POCl_3$ gettering step (see Fig. 5(a), for samples that were previously subjected to TR in an $N_2$ or $O_2$ ambient, the $iV_{oc}$ remains almost constant or declined by less than 10 mV. In Fig. 5(b), all the high-resistivity samples subjected to either a $N_2$ or $O_2$ ambient TR processing step showed an increase in $iV_{oc}$ of 10–40 mV. This includes the sample that was annealed in $O_2$ ambient for 30 min, which showed a significant decrease in $iV_{oc}$ after the BB step. This indeed confirms that the decrease in $iV_{oc}$ for this sample after the BB step was likely due to contamination and not due to oxygen precipitates. For the $n$-type Cz Si samples annealed in $N_2$ and $O_2$ ambient during the TR processing step (see Fig. 5(c), the $iV_{oc}$ increased by 5–15 mV after the $POCl_3$ gettering. Therefore, we can conclude that the almost constant or modest increase in $iV_{oc}$ after the $POCl_3$ gettering step is possibly due to effective impurity gettering to the surface due to the annihilation of oxygen precipitate nuclei in all three types of samples during the TR treatment, regardless of the ambient. This is further justified by the fact that in all three types of control Cz Si samples that were not subjected to TR, the $iV_{oc}$ declined by several 100 mV such that it can no longer be measured on the Sinton instrument. Conversely, we can conclude that due to the presence of oxygen precipitates in the control samples (see discussion in Section III-B), the $POCl_3$ gettering step was unsuccessful in removing impurities from the Si bulk and simply acts as another harsh thermal treatment with results in a decline in $iV_{oc}$ [40]. Similar to the BB, the ambient used during the $POCl_3$ gettering may affect the oxygen precipitate nuclei growth. If an $N_2$ ambient was used instead of an $O_2$ ambient, oxygen precipitation may progress differently than if an $O_2$ ambient was used.

### D. Effect of Tabula Rasa on LID

Fig. 6(a) and (b) shows the minority carrier lifetime of both (a) low- and (b) high-resistivity $p$-type Cz Si, respectively, during dark-annealing and light soaking for samples that were subjected to TR in $O_2$ ambient for 10 or 30 min, $N_2$ ambient for 10 min, and samples that did not undergo TR. For comparison, Fig. 6(a) also shows the minority carrier lifetime for a LID experiment without prior TR and BB processing steps. The 1-min timepoint denotes the dark-annealing minority carrier lifetime, and all subsequent time points are during light soaking (see Section II-C). Fig. 6 shows that for both samples, the minority carrier lifetime increases by at least a factor of two within the first 10 min of illumination if the samples were subjected to a prior TR processing step. After ~100 min of illumination, the minority carrier lifetime decreases, and reaches roughly the same level (at an injection level of $10^{15}$ cm$^{-3}$) that was recorded for the dark-annealed samples. For the low resistivity $p$-type Cz samples (see Fig. 6(a), after about the 3–6 h of illumination, the minority carrier lifetime increases slightly and then decreases again as the illumination is extended to 24 h. In comparison, the control sample that did not undergo TR treatment, but did undergo the boron emitter thermal budget
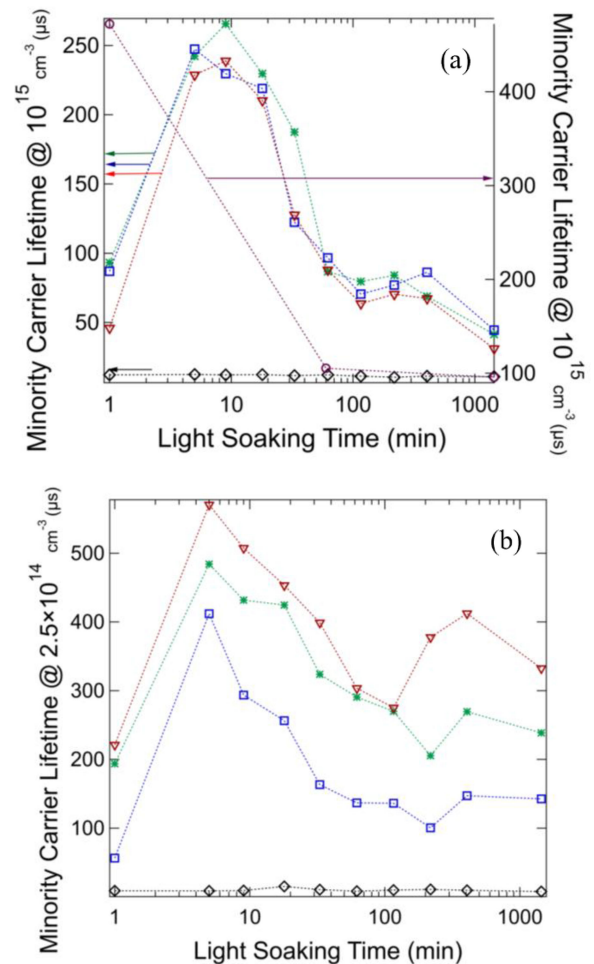


Fig. 6. Minority carrier lifetime as a function of light soaking time for (a) low-resistivity and (b) high-resistivity p-type Cz Si samples for the three different TR processes including $O_2$ ambient for 30 min (□), $O_2$ ambient for 10 min (*), and $N_2$ ambient for 10 min (▽). A control sample is also shown that did not undergo TR treatment (◇). In each case, the data point at 1 min represents the minority carrier lifetime after dark annealing at 200 °C for 20 min. All subsequent data pints were recorded during light soaking under 1 Sun for 24 h. The light-soaking data are also shown in (a) for a sample that did not undergo TR or BB processing steps (○). The dashed lines are a guide to the eye.

and $POCl_3$ gettering has a very low minority carrier lifetime ($<10$ $\mu$s) after dark annealing. Furthermore, unlike samples that were subjected to various TR treatments, we see that there is no change in the minority carrier lifetime for the control sample during the 24-h light-soaking period. We attribute this to the severe process-induced degradation of the control sample during the BB and $POCl_3$ gettering. Due to this prior degradation, the control sample's minority carrier lifetime is no longer limited by boron–oxygen defects that cause LID [9], [54], but due to other defects created in bulk Si at high temperatures. Typically, the minority carrier lifetime of boron-doped Cz-Si decreases exponentially when the dark-annealed samples undergo carrier injection such as under strong illumination [18]. This behavior is also shown in Fig. 6(a), which is very different than for the samples that were subjected to a prior TR processing step. The light soaking behavior after the TR step has not been reported previously. LID in boron-doped Cz-Si is attributed to

the formation of a $B_sO_{2i}$ complex that involves a substitutional boron atom ($B_s$) and an oxygen dimer ($O_{2i}$). Our data clearly show that the TR step eliminates the interstitial oxygen nuclei that lead to lifetime-limiting oxygen precipitates. Therefore, we hypothesize that the change in the interstitial oxygen bonding modifies the formation of the $B_sO_{2i}$ complex under illumination. Therefore, we predict that if a TR step is included in solar cell manufacturing, LID and regeneration protocols may have to be significantly modified.

As discussed above, Fig. 6 shows the evolution of the minority carrier lifetime as a function of the light-soaking time, which shows an initial maximum at ∼10 min and a second local maximum after 3–6 h of illumination. This suggests that there may be two different defects limiting the minority carrier lifetime over the 24-h light-soaking period. In order to rule out Fe-B pair dissolution at the beginning of light-soaking, samples were flashed with a Sinton lifetime tester ten times after LID experiments. The minority carrier lifetime did not increase and remained within a few microseconds before and after illumination. The injection level utilized to check for the presence of Fe-B pairs was $10^{15}$ cm$^{-3}$ and there was no systematic change in the minority carrier lifetime during the Fe-B test. We can interpret the presence of two defects by comparing the minority carrier lifetime curves recorded after ∼6 h of light soaking with those recorded during initial stages of light soaking. Fig. 7(a) shows the minority carrier lifetime as a function of the carrier injection level [55] after 5 min, 1, 6, and 24 h of light-soaking for the high-resistivity *p*-type Cz Si samples annealed in an $N_2$ ambient. In Fig. 7(a), while the absolute value of the minority carrier lifetimes is different after 5 min, 1 h, and 24 h, all three curves have nominally the same shape across a wide range of carrier injection levels. Conversely, the shape of the minority carrier lifetime curve recorded after 6 h differs significantly from minority carrier lifetime curves recorded 5 min, 1 h, and 24 h of illumination. In the low injection regime ($<10^{15}$ cm$^{-3}$), which is dominated by the SRH recombination, the slope of the minority carrier lifetime curve recorded after 6 h is different than the minority carrier lifetime curves recorded after 5 min, 1 h, and 24 h of light soaking. At $10^{15}$ cm$^{-3}$ carrier injection level, the minority carrier lifetimes recorded after 1 and 6 h of light soaking are nearly the same. Additionally, even though the maximum minority carrier lifetimes are also similar after 1 and 6 h of light-soaking, the maximum of the minority carrier lifetime recorded after 6 h is at an injection level of ∼5 × 14 cm$^{-3}$ while the maximum of the minority carrier lifetime recorded after 1 h is at ∼2 × 15 cm$^{-3}$. These differences in the minority carrier lifetime curves recorded in the initial stages and 6 h after light-soaking leads us to hypothesize that a different defect is limiting the minority carrier lifetime at the 6 h time point compared to the 5 min, 1 h, and 24 h time points.

In order to further investigate the hypothesis of two defects governing the minority carrier lifetime during light-soaking, the saturation current density $J_0$ was [56] extracted at an injection level of $10^{16}$ cm$^{-3}$ using the Sinton lifetime instrument with an intrinsic carrier concentration ($n_i$) of $1.5 \times 10^{10}$ cm$^{-3}$. We find that throughout the light-soaking process $J_0$ did not vary
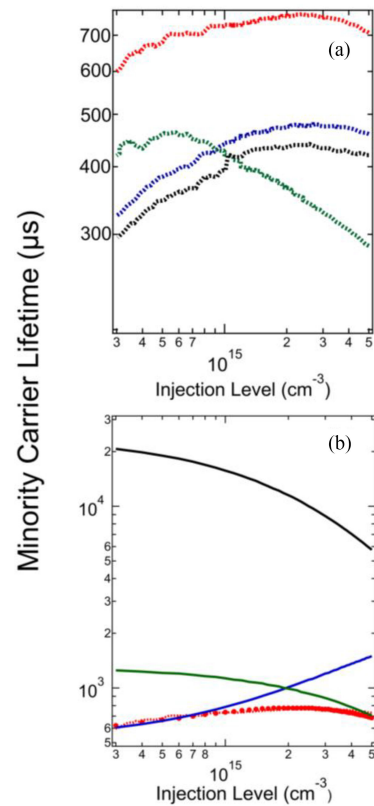


Fig. 7. (a) Minority carrier lifetime versus the injection level curve after 5 min (- - -), 1 h (- - -), 6 h (- - -), and 24 h (- - -) of light soaking at 1 Sun at room temperature for high-resistivity *p*-type Cz Si sample that was annealed in $N_2$ ambient for 10 min. (b) Minority carrier lifetimes shown in (a) for 5 min of light-soaking (- - -) and modeled lifetime curve after 5 min (•), including Auger (—), SRH (—), and surface (—) contributions for the modeling of the minority carrier lifetime after 5 min of light-soaking.

significantly. Additionally, the minority carrier lifetimes curves were fitted (see Fig. 7(b) for fitting for 5 min of light-soaking). To fit these curves, we took into account the Shockley–Read–Hall, Auger, and radiative recombination terms, using the same $n_i$ value of $1.5 \times 10^{10}$ cm$^{-3}$ [57]. The expression for the surface recombination term was based on Krügener *et al.* [58]. Fig. 7(b) shows the fitted minority carrier lifetime for the 5 min light-soaking time point. The parameters that were fitted were $J_0$, the trap density $N_t$, and the capture cross-section ratio $k$ for the Shockley–Read–Hall defect. We find that during the light-soaking process, we do not see substantial changes in $J_0$ regardless of whether it was obtained from Sinton measurements or from the fits in Fig. 7(b). However, even small changes in $J_0$ could result in substantial changes in the inverse lifetime if $J_0$ term is dominating the minority carrier lifetime curve. Since the changes in $J_0$ do not correlate with the effective lifetime, it gives us confidence that change in the minority carrier lifetime is due to a bulk defect and not a surface contribution. For comparison, the values of $J_0$ and $k$ obtained from the Sinton measurements and fitting are summarized in Table I. These results support our hypothesis that a different type of defect governs the lifetime at the initial and 6 h timepoints.

TABLE I
SUMMARY OF MODELED PARAMETERS

| Light-Soaking Time (Hr) | $J_0$ (Sinton) (fA/cm$^2$) | $J_0$ (model) (fA/cm$^2$) | $k$ (model) |
|---|---|---|---|
| 0.083 | 4 | 3 | 10 |
| 1 | 8 | 4 | 10 |
| 6 | 20 | 10 | 0.2 |
| 24 | 6 | 3 | 10 |

## IV. CONCLUSION

We have shown that conducting TR in an $O_2$ ambient results in an increase in the minority carrier lifetime compared to samples annealed in an $N_2$ ambient. We attribute this to Si interstitial injection during the $O_2$ TR treatment, effectively suppressing the vacancy and multivacancy formation. Additionally, we have shown that a TR processing step in either ambient, prior to a boron emitter thermal budget, can retard oxygen precipitation in both $n$-type and $p$-type Cz Si, and thus mitigate process-induced degradation by dissolving oxygen precipitate nuclei: this boron emitter thermal budget is an extremely harsh process, and harsher than any industrial processes for $p$-PERC solar cells. Both low- and high-resistivity $p$-type Cz Si samples treated in either an $O_2$ or $N_2$ ambient show no "ring-like" structures in PL images, which indicates that the TR pretreatment was successful in retarding the formation of lifetime-limiting oxygen precipitates. We can conclude from this that even with extremely harsh processing conditions, samples that underwent TR prior to the boron emitter thermal budget are generally immune to process-induced degradation brought on by oxygen precipitation. We have effectively made $p$-type Cz Si similar to float zone wafers, which do not have a large amount of oxygen in their bulk. Samples with no TR treatment show significant process-induced degradation, which manifests in the form of a dark PL image and the appearance of "ring-like" structures. Additionally, we show that subsequent $POCl_3$ gettering increased $iV_{oc}$ of all samples except low-resistivity $p$-type Cz Si and control samples. Finally, we show that the introduction of a TR processing step prior to light-soaking of boron-doped Cz Si, the trend in the minority carrier lifetime under illumination after dark annealing is modified. We attribute this to the change in the interstitial oxygen bonding in bulk Si and hypothesize that there is a second, transitory defect that governs the minority carrier lifetime at the 6 h light-soaking timepoint. This implies that if a TR step is incorporated into $p$-PERC cell manufacturing, the regeneration step after LID would have to be better understood and reoptimized accordingly.

## ACKNOWLEDGMENT

## REFERENCES

[1] T. Dullweber and J. Schmidt, "Industrial silicon solar cells applying the passivated emitter and rear cell (PERC) concept—A review," *IEEE J. Photovolt.*, vol. 6, no. 5, pp. 1366–1381, Sep. 2016.

[2] M. A. Green, "The passivated emitter and rear cell (PERC): From conception to mass production," (in English), *Sol. Energy Mater. Sol. Cells*, vol. 143, pp. 190–197, 2015.

[3] M. A. Green, *High Efficiency Silicon Solar Cells* (Materials Science Surveys). Brookfield, VT, USA: Aedermannsdorf, Switzerland: Trans Tech Publications, 1987.

[4] A. W. Blakers, A. Wang, A. M. Milne, J. H. Zhao, and M. A. Green, "22.8-percent efficient solar cell," *Appl. Phys. Lett.*, vol. 55, no. 13, pp. 1363–1365, 1989.

[5] M. A. Green, A. W. Blakers, J. Shi, E. M. Keller, and S. R. Wenham, "19.1-percent efficient solar cell," *Appl. Phys. Lett.*, vol. 44, no. 12, pp. 1163–1164, 1984.

[6] V. LaSalvia *et al.*, "*Tabula Rasa* for n-Cz silicon-based photovoltaics," *Prog. Photovolt.*, vol. 27, pp. 136–143, 2018.

[7] A. Borghesi, B. Pivac, A. Sassella, and A. Stella, "Oxygen precipitation in silicon," *J. Appl. Phys.*, vol. 77, no. 9, pp. 4169–4244, 1995.

[8] M. Pagani, R. J. Falster, G. R. Fisher, G. C. Ferrero, and M. Olmo, "Spatial variations in opygen precipitation in silicon after high temperature readip thermal annealing," *Appl. Phys. Lett.*, vol. 70, 1997, Art. no. 1572.

[9] J. D. Murphy, R. E. McGuire, K. Bothe, V. V. Voronkov, and R. J. Falster, "Minority carrier lifetime in silicon photovoltaics: The effect of oxygen precipitation," *Sol. Energy Mater. Sol. Cells*, vol. 120, pp. 402–411, 2014.

[10] D. C. Walter, B. Lim, R. Falster, J. Binns, and J. Schmidt, "Understanding degradation in Czochralski-grown n-type silicon after high-temperature processing," in *Proc. 28th Eur. Photovolt. Sol. Energy Conf.*, Paris, France, 2013, pp. 699–702.

[11] K. F. Kelton, *et al.* "Oxygen precipitation in silicon: Experimental studies and theoretical investigations within the classical theory of nucleation," *J. Appl. Phys.*, vol. 85, 1999, Art. no. 8097.

[12] J. D. Murphy, K. Bothe, M. Olmo, V. V. Voronkov, and R. J. Falster, "The effect of oxide precipitates on minority carrier lifetime in p-type silicon," *J. Appl. Phys.*, vol. 110, no. 5, 2011, Art. no. 9.

[13] F. Wolny, T. Weber, M. Muller, and G. Fischer, "Light induced degradation and regeneration of high efficiency Cz PERC cells with varying base resistivity," *Energy Procedia*, vol. 38, pp. 523–530, 2013.

[14] J. Schmidt and K. Bothe, "Structure and transformation of the metastable boron- and oxygen-related defect center in crystalline silicon," *Physical Rev. B*, vol. 69, no. 2, 2004, Art. no. 8.

[15] K. Bothe and J. Schmidt, "Electronically activated boron-oxygen-related recombination centers in crystalline silicon," *J. Appl. Phys.*, vol. 99, no. 1, 2006, Art. no. 11.

[16] A. Herguth, G. Schubert, M. Kaes, and G. Hahn, "A new approach to prevent the negative impact of the metastable defect in boron doped Cz silicon solar cells," in *Proc. IEEE 4th World Conf. Photovolt. Energy Convers.*, Waikoloa, HI, USA, 2006, pp. 940–943.

[17] B. Hallam *et al.*, "Eliminating light-induced degradation in commercial p-type Czochralski silicon solar cells," *Appl. Sci.-Basel*, vol. 8, no. 1, 2018, Art. no. 19.

[18] K. Bothe, R. Sinton, and J. Schmidt, "Fundamental boron-oxygen-related carrier lifetime limit in mono- and multicrystalline silicon," *Prog. Photovolt.*, vol. 13, no. 4, pp. 287–296, 2005.

[19] H. Yamanaka, Y. Aoki, and T. Samizo, "Role of silicon self-interstitials injected by thermal-oxidation in oxygen precipitation in Czochralski silicon," *Jpn. J. Appl. Phys.*, vol. 29, no. 11, pp. 2450–2455, 1990.

[20] S. M. Hu, "Precipitation of oxygen in silicon—some phenomena and a nucleation model," *J. Appl. Phys.*, vol. 52, no. 6, pp. 3974–3984, 1981.

[21] C. Y. Kung, "Effect of thermal history on oxygen precipitates in zochralski silicon anneale at 1050-degrees-C," *J. Appl. Phys.*, vol. 65, no. 12, pp. 4654–4665, 1989.

[22] K. Yasutake *et al.*, "Oxygen-related donors generated at 800-degrees-C in Cz-Si," *Jpn J. Appl. Phys.*, vol. 19, no. 9, pp. L544–L546, 1980.

[23] N. Inoue, J. Osaka, and K. Wada, "Oxide micro-precipitates in as-grown Cz silicon," *J. Electrochemical Soc.*, vol. 129, no. 12, pp. 2780–2788, 1982.

[24] C. Y. Kung, L. Forbes, J. D. Peng, W. M. Bullis, and L. C. Kimerling, Eds. *Defects in Silicon*. Pennington, NJ, USA: Electrochemical Society, 1983.

[25] S. M. Hu, "Effects of ambeints on oxygen precipitation in silicon," *Appl. Phys. Lett.*, vol. 36, no. 7, pp. 561–564, 1980.

[26] G. S. Oehrlein, J. L. Lindstrom, and J. W. Corbett, "Carbon-oxygen complexes as nuclei for the precipitation of oxygen in Czochralski silicon," *Appl. Phys. Lett.*, vol. 40, no. 3, pp. 241–243, 1982.

[27] A. Borghesi, B. Pivac, and A. Sassella, "Oxygen precipitates in short-time annealed Czochralski silicon," *J. Cryst. Growth*, vol. 126, no. 1, pp. 63–69, 1993.

[28] H. Furuya, I. Suzuki, Y. Shimanuki, and K. Murai, "Formation of nuclei of oxygen precipitates in Cz silicon-crystals during crystal-growth process," *J. Electrochemical Soc.*, vol. 135, no. 3, pp. 677–682, 1988.

[29] R. Basnet *et al.*, "Methods to improve bulk lifetime in n-type Czochralski-grown upgraded metallurgical-grade silicon wafers," *IEEE J. Photovolt.*, vol. 8, no. 4, pp. 990–996, Jul. 2018.

[30] M. Meduna, O. Caha, J. Kubena, A. Kubena, and J. Bursik, "Homogenization of CZ Si wafers by Tabula Rasa annealing," *Physica B-Condens. Matter*, vol. 404, no. 23/24, pp. 4637–4640, 2009.

[31] D. C. Walter *et al.*, "Effect of rapid thermal annealing on recombination centres in boron-doped Czochralski-grown silicon," *Appl. Phys. Lett.*, vol. 104, 2014, Art. no. 042111.

[32] W. Wijaranakula, "The dissolution mechanism of oxide precipitates in Czochralski silicon degenerately doped with boron during high-temperature annealing," *J. Electron. Mater.*, vol. 22, no. 1, pp. 105–110, 1993.

[33] W. Wijaranakula, "Morphology of oxide precipitates in Czochralski silicon degenerately doped with boron," *J. Appl. Phys.*, vol. 72, no. 9, pp. 4026–4030, 1992.

[34] R. Murray *et al.*, "Interlaboratory determination of oxygen in silicon for certified reference materials," *J. Electrochemical Soc.*, vol. 139, no. 12, pp. 3582–3587, 1992.

[35] W. Kern and D. A. Puotinen, "Cleaning solutions based on hydrogen peroxide for use in silicon semiconductor technology," *RCA Rev.*, vol. 31, no. 2, 1970, Art. no. 187.

[36] K. Reinhardt, W. Kern, and W. Andrew, Ed. *Handbook of Silicon Wafer Cleaning Technology*, 2nd ed. Norwich, NY, USA: William Andrew Inc., 2008.

[37] C. A. Londos, M. J. Binns, A. R. Brown, S. A. McQuaid, and R. C. Newman, "Effect of oxygen concentration on the kinetics of thermal donor formation in silicon at temperatures between 350 °C and 500 °C," *Appl. Phys. Lett.*, vol. 62, no. 13, pp. 1525–1526, 1993.

[38] M. Claybourn and R. C. Newman, "Thermal donor formation and the loss of oxygen from solution in silicon heated at 450 °C," *Appl. Phys. Lett.*, vol. 52, no. 25, pp. 2139–2141, 1988.

[39] B. Hallam, B. Tjahjono, T. Trupke, and S. Wenham, "Photoluminescence imaging for determining the spatially resolved implied open circuit voltage of silicon solar cells," *J. Appl. Phys.*, vol. 115, 2014, Art. no. 044901.

[40] P. Pichler, *Intrinsic Point Defects, Impurities, and Their Diffusion in Silicon*. New York, NY, USA: Springer-Verlag Wien, 2004.

[41] F. E. Rougieux, H. T. Nguyen, D. H. Macdonald, B. Mitchell, and R. Falster, "Growth of oxygen precipitates and dislocations in Czochralski silicon," *IEEE J. Photovolt.*, vol. 7, no. 3, pp. 735–740, May 2017.

[42] R. Falster, V. V. Voronkov, and F. Quast, "On the properties of the intrinsic point defects in silicon: A perspective from crystal growth and wafer processing," *Physica Status Solidi (b)*, vol. 222, 2000, Art. no. 219.

[43] R. Falster *et al.*, "Vacancy-assisted oxygen precipitation phenomena in Si," *Solid State Phenomena*, vol. 57–58, pp. 129–136, 1997.

[44] D. A. Antoniadis, "Oxidation-induced point-defects in silicon," *J. Electrochemical Soc.*, vol. 129, no. 5, pp. 1093–1097, 1982.

[45] T. Y. Tan and U. Gosele, "Growth-kinetics of oxidation-induced stacking-faults in silicon—A new concept," *Appl. Phys. Lett.*, vol. 39, no. 1, pp. 86–88, 1981.

[46] D. A. Antoniadis and I. Moskowitz, "Diffusion of substitutional impurities in silicon at short oxidation times - An insight into point-defect kinetics," *J. Appl. Phys.*, vol. 53, no. 10, pp. 6788–6796, 1982.

[47] D. Skarlatos, M. Omri, A. Claverie, and D. Tsoukalas, "Estimation of the number of interstitial atoms injected in silicon during thin oxide formation," *J. Electrochemical Soc.*, vol. 146, no. 6, pp. 2276–2283, 1999.

[48] D. F. Downey, M. Farley, K. S. Jones, and G. Ryding, *Ion Implantation Technology-92*. Amsterdam, The Netherlands: North Holland Elsevier B.V., 1993.

[49] M. N. Kham, I. Matko, B. Chenevier, and P. Ashburn, "Reduced boron diffusion under interstitial injection in fluorine implanted silicon," *J. Appl. Phys.*, vol. 102, no. 11, pp. 7, 2007.

[50] Q. Wei, F. Miao, W. Lian, H. Qian, and Z. Ni, "Optimization of light induced degradation regeneration of p-type mono PERC solar cell by electrical injection method," in *Proc. AIP Conf.*, 2018, vol. 1999, pp. 110008-1–110008-5.

[51] B. Hallam *et al.*, "The role of hydrogenation and gettering in enhancing the efficiency of next-generation Si solar cells: An industrial perspective," *Physica Status Solidi a-Appl. Mater. Sci.*, vol. 214, no. 7, 2017, Art. no. 1700305.

[52] D. P. Fenning *et al.*, "Improved iron gettering of contaminated multicrystalline silicon by high-temperature phosphorus diffusion," *J. Appl. Phys.*, vol. 113, no. 21, 2013, Art. no. 214504.

[53] G. Kissinger *et al.*, "Investigation of the copper gettering mechanism of oxide precipitates in silicon," *ECS J. Solid State Sci. Technol.*, vol. 4, no. 9, pp. N124–N129, 2015.

[54] J. D. Murphy, R. E. McGuire, K. Bothe, V. V. Voronkov, and R. J. Falster, "Competitive gettering of iron in silicon photovoltaics: Oxide precipitates versus phosphorus diffusion," *J. Appl. Phys.*, vol. 116, no. 5, 2014, Art. no. 053514.

[55] R. A. Sinton and A. Cuevas, "Contactless determination of current-voltage characteristics and minority-carrier lifetimes in semiconductors from quasi-steady-state photoconductance data," *Appl. Phys. Lett.*, vol. 69, no. 17, pp. 2510–2512, 1996.

[56] A. W. Blakers and M. A. Green, "Oxidation condition dependence of surface passivation in high efficiency silicon solar cells," *Appl. Phys. Lett.*, vol. 47, pp. 818–820, 1985.

[57] M. Z. Rahman, "Modeling minortiy carrier's recombination lifetime of p-Si solar cell," *Int. J. Renewable Energy Res.*, vol. 2, pp. 117–122, 2012.

[58] J. Krügener, F. Haase, M. Rienäcker, R. Brendel, H. J. Osten, and R. Peibst, "Improvement of SRH bulk lifetime upon formation of n-type POLO junctions for 25% efficient Si solar cells," *Sol. Energy Mater. Sol. Cells*, vol. 173, pp. 85–91, 2017.